Pathogenic CD8 T cell responses are driven by neutrophil-mediated hypoxia in cutaneous leishmaniasis

Erin A. Fowler[1], Camila Farias Amorim[2], Klauss Mostacada[1], Allison Yan[1], Laís Amorim Sacramento[2], Rae A. Stanco[1], Emily D. S. Hales[1], Aditi Varkey[1], Wenjing Zong[3]†, Gary D. Wu[3], Camila I. de Oliveira[4], Patrick L. Collins[1], Fernanda O. Novais[1]*

[1]Department of Microbial Infection and Immunity, College of Medicine, The Ohio State University; Columbus, USA

[2]Department of Pathobiology, School of Veterinary Medicine, University of Pennsylvania; Philadelphia, USA

[3]Division of Gastroenterology and Hepatology, Perelman School of Medicine, University of Pennsylvania; Philadelphia, USA.

[4]Centro de Pesquisas Gonçalo Moniz, Fundação Oswaldo Cruz, Salvador, Brazil

†Current address: Division of Gastroenterology/Hepatology/Nutrition, Children's Hospital of Philadelphia; Philadelphia, USA.

*Corresponding author:

Fernanda O. Novais
The Ohio State University, College of Medicine
720 BRT 460 W 12th Ave
Columbus OH 43210
+1 614 366 9272
Email: Fernanda.Novais@osumc.edu

Conflict of Interest: The authors have declared no conflict of interest exists.

Abstract

Cutaneous leishmaniasis caused by *Leishmania* parasites exhibits a wide range of clinical manifestations. Although parasites influence disease severity, cytolytic CD8 T cell responses mediate disease. While these responses originate in the lymph node, we find that expression of the cytolytic effector molecule granzyme B is restricted to lesional CD8 T cells in *Leishmania*-infected mice, suggesting that local cues within inflamed skin induce cytolytic function. Expression of Blimp-1 (*Prdm1*), a transcription factor necessary for cytolytic CD8 T cell differentiation, is driven by hypoxia within the inflamed skin. Hypoxia is further enhanced by the recruitment of neutrophils that consume oxygen to produce reactive oxygen species, ultimately increasing granzyme B expression in CD8 T cells. Importantly, lesions from cutaneous leishmaniasis patients exhibit hypoxia transcription signatures that correlate with the presence of neutrophils. Thus, targeting hypoxia-driven signals that support local differentiation of cytolytic CD8 T cells may improve the prognosis for patients with cutaneous leishmaniasis, as well as other inflammatory skin diseases where cytolytic CD8 T cells contribute to pathogenesis.

42 **INTRODUCTION**

43

44 Cutaneous leishmaniasis is caused by *Leishmania* parasites and exhibits a wide range of
45 clinical manifestations, from self-healing lesions to chronic debilitating infections *(1)*. No
46 vaccines exist for leishmaniasis, and the anti-parasitic drugs are often ineffective *(2)*. Although
47 the parasites influence disease severity, immune responses are often the major driver of disease.
48 For example, CD8 T cells in lesions are recruited to target parasite-infected cells and kill infected
49 host cells through granule-mediated cytotoxicity. However, the destruction of infected cells does
50 not kill *Leishmania*, but leads to the release of parasites that metastasize to distant cutaneous
51 sites *(3)*. In addition, cell death induced by CD8 T cells activates the NLRP3 inflammasome, IL-
52 1β release, chronic neutrophil recruitment, and enhanced inflammation *(3–6)*. The importance of
53 this pathway is supported by our previous analysis of lesions from patients, in which granzyme B
54 (*GZMB*), perforin (*PRF1*), and *IL1B* expression were associated with treatment failure *(7)*. While
55 both murine and human studies underscore the pathogenic consequences of cytotoxicity, the
56 microenvironmental cues and downstream mechanisms that drive cytolytic programs in lesional
57 CD8 T cells remain unknown.

58 In response to *Leishmania* infection, CD8 T cells are activated and expand in draining
59 lymph nodes (dLNs). The activated cells then travel to inflammatory sites, where they kill
60 infected cells. While infections also induce differentiation of effector CD4 T cells in secondary
61 lymphoid organs, CD8 T cells with cytotoxic effector function are generally absent in LNs (8–
62 11). A prior study implicated PD-1 ligation on dLN CD8 T cells in suppressing their expression
63 of granzyme B, a process that is likely advantageous since it would limit the killing of antigen-
64 presenting cells (11). While such findings suggest that CD8 T cell cytolytic effector function is

65 only triggered once CD8 T cells enter inflammatory sites (12, 13), the local cues that drive this
66 response remain unclear. As the CD8 T cell cytolytic program can have both positive and
67 negative consequences for the host (14–33), understanding the mechanisms that drive cytotoxic
68 CD8 T cell programs remains an important goal for unraveling pathogenesis of numerous
69 diseases such as alopecia, vitiligo, bullous pemphigoid, Steven-Johnson syndrome and toxic
70 epidermal necrolysis, where cytolytic CD8 T cells contribute to pathogenesis (15, 32, 34–37).
71 One potential mechanism relevant to inflamed tissues is hypoxia, which occurs when
72 oxygen consumption by infiltrating cells exceeds the supply (38) and differentially impacts
73 immune cell types. In *Leishmania* infection, hypoxia has been studied exclusively in
74 macrophages and dendritic cells (39, 40), where it can either promote or block effector
75 responses, depending on the parasite species and the cell type (41–49). Here, we find that
76 hypoxia within *Leishmania*-infected lesions directly promotes cytolytic effector function in
77 newly recruited CD8 T cells. Mechanistically, we identify a feed-forward loop, initiating with
78 early recruitment of neutrophils that consume oxygen to produce reactive oxygen species (ROS),
79 which promotes a persistently hypoxic environment, elevates the number of cytolytic CD8 T
80 cells, perpetuates chronic neutrophil recruitment, and exacerbates tissue damage. Thus, our
81 findings indicate that targeting cytolytic CD8 T cells driven by hypoxic microenvironments will
82 improve the prognosis for patients with cutaneous leishmaniasis and other inflammatory skin
83 diseases.

84

85 **RESULTS**

86

87 **CD8 T cells express granzyme B in leishmanial lesions but not in the draining lymph nodes.**

88

89 Cytotoxic CD8 T cells are pathogenic in cutaneous leishmaniasis (3, 4, 6, 7, 50–54), but
90 their anatomical distribution and mechanisms that regulate their induction remain unclear. In this
91 regard, parasites are found in both dLNs and skin lesions. To determine if CD8 T cell cytotoxic
92 effector function is present in both tissues, we assessed the expression of the cytotoxic marker
93 granzyme B. C57BL/6 mice were infected with *Leishmania* in the ear, and two weeks post-
94 infection, the frequency of granzyme B^{pos} antigen-experienced ($CD44^{high}$) CD8 T cells was
95 assessed by flow cytometry. While granzyme B-expressing CD8 T cells were abundant in the
96 infected skin, granzyme B expression was nearly absent in dLNs (Fig 1a). To determine if
97 granzyme B^{pos} CD8 T cells were preferentially recruited to the skin, we treated mice with
98 FTY720, a sphingosine 1-phosphate receptor agonist that blocks the egress of T cells from the
99 dLNs. If granzyme B^{pos} CD8 T cells are preferentially recruited to cutaneous lesions, granzyme
100 B^{pos} CD8 T cells should accumulate in the dLNs of FTY720-treated mice. However, there was
101 no difference in the frequency of granzyme B^{pos} CD8 T cells in the dLNs of mice treated with
102 FTY720 or vehicle control (Fig. 1b), suggesting that rather than preferential recruitment,
103 exposure to the lesion microenvironment induces a cytotoxic profile in CD8 T cells. To directly
104 test this, we infected C57BL/6 CD45.1 or CD45.2 congenic mice with *Leishmania*, and purified
105 CD8 T cells from dLNs of CD45.2 donor mice (granzyme B^{neg}) three weeks post-infection.
106 Donor dLN CD8 T cells were then transferred directly into the lesions of recipient CD45.1
107 infected animals (Fig. 1c - schematic). Notably, we found that granzyme B^{neg} CD8 T cells
108 became granzyme B-expressing CD8 T cells in the lesions (Fig. 1c). In contrast, CD8 T cells that
109 migrated back to dLNs remained granzyme B^{neg} (Fig. 1c). These results demonstrated that the
110 lesion microenvironment triggers cytotoxic programs in CD8 T cells.

111

112 To determine the mechanisms by which CD8 T cell cytotoxic programs are induced in
113 lesions, we performed RNA-seq analysis on purified antigen-experienced CD8 T cells from
114 dLNs and lesions of mice infected with *Leishmania* for five weeks. Principal component analysis
115 (PCA) showed that almost half (Principal component 1, PC1 47%) of the differences on the
116 whole transcriptional profiles were associated with the organ from which the CD8 T cells were
117 derived (Fig. 1d). Differentially expressed gene (DEG) analysis with thresholds of false
118 discovery rate (FDR) < 0.05 and fold change > 1.5 between tissues revealed 118 genes
119 overexpressed in CD8 T cells from lesions compared to dLNs and 26 DEGs overexpressed in
120 dLNs compared to lesions (Supp. Table 1 and Suppl. Fig. 1). *Gzmb* was the top DEG in CD8 T
121 cells from lesions compared to dLNs, FDR=0.002 (Fig. 1e). Several transcription factors play
122 important roles in effector CD8 T cell biology, including BATF, ID-2, IRF4, Stat4, T-bet, Zeb2,
123 and Blimp-1 (encoded by *Prdm1*) (55–57), and we found that *Id2*, *Irf4*, and *Prdm1* expressions
124 were significantly higher in lesions than in dLNs, and *Prdm1* had the most significant fold
125 change between tissues (>100 higher in lesions) (Fig. 1f). To further investigate the signals
126 received by CD8 T cells within lesions, we performed Gene Set Enrichment Analysis (GSEA),
127 which exhibited hypoxia-related signatures, as assessed by several pathway databases (Hallmark,
128 Biocarta, and Reactome), as well as the Harris et al. hypoxia-specific pathway described in (58),
129 (Fig. 1g and Supp. Table 2). These data indicate that, after their exit from dLNs, CD8 T cells
130 recruited to cutaneous leishmaniasis lesions are exposed to hypoxic conditions, inducing the
131 expression of key cytotoxicity effector mediators, including *Prdm1*.

132

133 **Cutaneous leishmaniasis lesions are hypoxic and alter CD8 T cell function.**

134

135 Normal skin is naturally low in oxygen (59, 60), and inflammatory environments are
136 frequently hypoxic. To evaluate hypoxia in *Leishmania*-infected lesions, we employed
137 pimonidazole, a 2-nitroimidazole reporter molecule that is reductively activated and forms
138 covalent bonds with macromolecules, specifically in hypoxic cells. Mice were injected with
139 pimonidazole two weeks after *Leishmania* infection and one hour before euthanasia.
140 Pimonidazole staining was assessed in infected and contralateral ears by confocal microscopy.
141 As expected, we found pimonidazole staining within the epidermis, dermis, and hair follicles of
142 naïve mice (Fig. 2a and 2b – top images). Within lesions, we observed enlargement of the
143 epidermis and dermis associated with robust pimonidazole staining (Fig. 2a and 2b – bottom
144 images). Surprisingly, pimonidazole staining was absent from ulcerated areas. Representative
145 images in lower (Fig. 2a and Supp. Fig. 2a) and higher (Fig. 2b and Supp. Fig. 2b) magnification
146 depict the differences in pimonidazole staining distribution between the naïve and infected
147 tissue.

148 To compare O_2 levels in lesions and dLNs, we infected mice with *Leishmania,* and two
149 weeks post-infection, mice received Oxyphor G4, a phosphorescent probe quenched by oxygen
150 (61). Infected skin exhibited a significant decrease in oxygen compared to dLNs (Fig. 2c). These
151 data directly demonstrated skin lesions present a hypoxic microenvironment to CD8 T cells upon
152 their recruitment from dLNs.

153 We tested whether exposure to hypoxia was sufficient to promote granzyme B expression
154 in dLN CD8 T cells. We isolated dLN cells from infected mice and stimulated them with anti-
155 CD3 and anti-CD28 in the presence of Dimethyloxalylglycine (DMOG), a compound that
156 mimics hypoxia at normal oxygen tension. As shown in Fig. 2d, DMOG induced the expression

157 of granzyme B in CD8 T cells, further demonstrating that hypoxia promotes upregulation of their
158 cytolytic program. Notably, DMOG treatment also increased *Prdm1* mRNA expression
159 compared to vehicle-treated CD8 T cells (Fig. 2e). Collectively, these data demonstrate that the
160 hypoxic state of lesions stimulates differentiation of recruited CD8 T cells into cytotoxic
161 effectors.

162

163 **Blimp-1 expression is restricted to granzyme B expressing CD8 T cells.**

164

165 Blimp-1 deficient CD8 T cells produce less granzyme B (62), so we next sought to test
166 cause-effect relationships between hypoxia, Blimp-1, and cytotoxicity. To address this question,
167 we infected Blimp-1 Yellow Fluorescent Protein (YFP) reporter mice with *Leishmania* and
168 assessed Blimp-1 expression in CD8 T cells. We found that Blimp-1 was highly expressed in
169 lesional CD8 T cells but not in CD8 T cells from the dLNs (Fig. 3a). We also found that Blimp-1
170 expression was significantly higher in CD8 T cells that express granzyme B (Fig. 3b), suggesting
171 a link between Blimp-1 and cytotoxicity. Finally, to assess if granzyme B expression in lesions
172 resulted from hypoxic induction of Blimp-1, we used mice expressing a fusion protein bearing an
173 oxygen-dependent degradation (ODD) domain from human HIF1A (hypoxia-inducible factor 1,
174 alpha subunit) fused to a tamoxifen-inducible Cre recombinase gene (cre/ERT2) (63). When
175 expressed under normoxic conditions, the O2CreER fusion protein is degraded rapidly but is
176 stabilized by hypoxia when combined with tamoxifen injection. These mice were crossed with
177 Blimp-1$^{flox/flox}$ mice (here called ODD^{cre}Blimp-1$^{flox/flox}$ mice) to generate mice in which Blimp-1
178 expression is deleted specifically in hypoxic cells upon tamoxifen injection (Fig. 3c). Since the
179 skin has significantly less oxygen than dLNs, these mice provide lesion-specific deletion of

180 Blimp-1, thus ensuring the preservation of Blimp-1-dependent development of effector T cells in
181 dLNs (normoxic) and their recruitment to the inflamed tissue. *Leishmania*-infected
182 ODD^{cre}Blimp-1$^{flox/flox}$ mice were treated with tamoxifen or left untreated for one week, and
183 granzyme B expression was evaluated. We found that specific deletion of Blimp-1 in hypoxic
184 cells significantly decreased granzyme B expression in lesional CD8 T cells compared to
185 untreated mice (Fig. 3d). Taken together, these results directly demonstrate that upregulation of
186 Blimp-1 by the hypoxic environment leads to increased granzyme B expression and CD8 T cell
187 cytotoxicity in leishmanial lesions.

188

189 **Blimp-1 expression is necessary for CD8 T cells to mediate disease.**

190

191 Based on our data, we predicted that Blimp-1 expression was required for cytotoxic CD8
192 T cell-mediated disease in leishmaniasis. Since Blimp-1 plays a vital role in CD4 T cell subsets
193 (64) and regulates IL-10 production (65), total T cell deletion of Blimp-1 would complicate
194 interpretations. Therefore, we used our well-characterized mouse model of chronic leishmaniasis
195 in which severe disease develops following *Leishmania* infection of RAG-deficient mice
196 reconstituted with CD8 T cells (3, 4, 66, 67). RAG-deficient mice infected with *Leishmania* were
197 reconstituted with WT or CD8 T cells lacking Blimp-1 expression (here called Blimp-1^{cKO}) or
198 control animals receiving no T cells. As described previously (3), RAG-deficient mice
199 reconstituted with WT CD8 T cells developed severe pathology characterized by granzyme B-
200 expressing CD8 T cells in lesions, while RAG-deficient mice that received no cells showed no
201 signs of pathology (Fig. 4a). Importantly, RAG-deficient mice reconstituted with Blimp-1^{cKO}
202 CD8 T cells had minimal disease (Fig. 4a). As expected, there were similar numbers of parasites

203 (Fig. 4b) and a similar frequency of CD8 T cells (Fig. 4c) in lesions of RAG-deficient mice
204 reconstituted with WT and Blimp-1^{cKO} CD8 T cells. Notably, granzyme B expression was
205 significantly diminished in cells lacking Blimp-1 (Fig. 4d). Collectively, these data indicate that
206 Blimp-1 expression is driven by the hypoxic microenvironment of the lesion, triggering
207 granzyme B expression and CD8 T cells-driven pathology.

208

209 **Neutrophils generate the hypoxic microenvironment of cutaneous leishmaniasis lesions**.

210

211 Hypoxia occurs in tissues when oxygen supply does not meet demand, including
212 scenarios characterized by defective tissue vascularization or increased demand by cells present
213 within a tissue (38). *Leishmania*-infected lesions are highly vascularized (68), so we
214 hypothesized that oxygen consumption by inflammatory cells recruited to cutaneous
215 leishmaniasis lesions promoted hypoxia. Neutrophils are the first cells recruited to skin upon
216 *Leishmania* infection (69), but their recruitment does not control *L. major* parasites. Indeed, their
217 chronic presence is associated with worsening disease (3, 4, 70–74). Therefore, we tested
218 whether neutrophil recruitment contributed to the hypoxic state of inflamed skin. *Leishmania*-
219 infected mice were injected with pimonidazole 1 hour before euthanasia at multiple time points
220 after infection: 1) soon after parasite challenge (2 and 5 hours), 2) when lesions started to
221 develop, and CD8 T cells were present and expressed granzyme B (2 weeks), and 3) when
222 lesions began to heal (9 weeks). As expected (69), neutrophils were quickly recruited to
223 *Leishmania*-infected lesions and decreased in frequency when lesions resolved (Fig. 5a).
224 Surprisingly, neutrophil (CD11b^{pos}Ly6G^{pos}) staining by pimonidazole was significantly lower
225 compared to other myeloid cells (CD11b^{pos}Ly6G^{neg}) in the skin at all time points analyzed (Fig.

226 5b). To confirm these observations, lesions from pimonidazole-injected mice were stained for
227 Ly6G (clone 1A8), revealing intense neutrophil recruitment in ulcered regions in the epidermis
228 and clusters of neutrophils within the skin dermis (Fig. 5c and Fig. S3a). Notably, regions
229 without neutrophils had significantly more pimonidazole staining than those containing
230 neutrophil clusters. We also observed that pimonidazole staining in regions surrounding
231 neutrophil clusters was more intense. Quantitative assessment of pixel intensities (Supp. Fig. 3b)
232 revealed a negative correlation between pimonidazole and Ly6G expression (Fig. 5d). Higher
233 magnification of regions with intense neutrophil recruitment at two different time points showed
234 a lack of pimonidazole staining in neutrophils (Fig. 5e and Supp. Fig. 3c).

235 These results suggest that areas surrounding neutrophils are relatively hypoxic.
236 Accordingly, we hypothesized that neutrophils were responsible for promoting the hypoxic state
237 of the skin by competing for oxygen, thereby controlling CD8 T cell-effector function. To test
238 this, we depleted mice of neutrophils for the first two weeks of infection using anti-Ly6G (clone
239 1A8) (Fig. 5f) at the early stage of disease development and assessed granzyme B expression in
240 CD8 T cells. We found that neutrophil depletion decreased the frequency and the mean
241 fluorescence intensity (MFI) of granzyme B expressing CD8 T cells compared to isotype
242 control-treated mice (Fig. 5g), without changing parasite numbers or lesion size (data not
243 shown). These data suggest that neutrophils consume oxygen in lesions, altering the phenotype
244 of CD8 T cells.

245

246 In this regard, activated neutrophils assemble NADPH oxidase to produce reactive
247 oxygen species (ROS), which requires oxygen (75). Thus, we tested whether oxygen
248 consumption to generate ROS resulted in a hypoxic state that impacted CD8 T cell function. For

249 this purpose, we compared the ability of mice sufficient (WT) or deficient in the gp91^{phox} subunit
250 of the NADPH oxidase (Cybb$^{-/-}$) to express granzyme B in lesional CD8 T cells upon infection
251 with *Leishmania*. We found significantly less granzyme B expressing CD8 T cells in Cybb$^{-/-}$
252 mice than in WT (Fig. 5h), forging a link between NADPH oxidase-dependent ROS production
253 and the development of pathogenic CD8 T cells in cutaneous leishmaniasis lesions.

254

255 **The magnitude of hypoxia correlates with the presence of neutrophils in human cutaneous**
256 **leishmaniasis lesions.**

257 To determine whether hypoxia is a feature of human disease, we compared
258 transcriptional signatures in blood and skin from healthy subjects (HS) and cutaneous
259 leishmaniasis (CL) patients using previously published datasets (51, 76). To estimate levels of
260 hypoxia-gene expression in clinical samples, we performed single-sample GSEA using the
261 Harris et al. hypoxia gene signature (58), and referred to this variable as the "hypoxia score"
262 (Supp. Table 3). While there was no difference in the hypoxia scores between blood from
263 cutaneous leishmaniasis patients and healthy subjects (Fig. 6a and Supp. Table 4), the cutaneous
264 leishmaniasis lesions are significantly more hypoxic than healthy skin (Fig. 6b, Data File S3).
265 Importantly, we observed that the degree of the hypoxia-related gene expression in patients'
266 lesions was variable. To understand the biological implication of this variability, we performed
267 unsupervised hierarchical clustering (HC) to classify lesions and healthy skin samples according
268 to their hypoxic gene expression accessed by Harris et al., Hallmark, Biocarta and Reactome
269 sources (Fig. 6c). HC analysis revealed two groups of lesion samples: (1) 'baseline' lesions (n =
270 22) with a hypoxia phenotype comparable to control skin samples, and (2) 'hypoxic' lesions (n =
271 12) with a high hypoxic phenotype relative to the entire cohort (Fig. 6b and Fig 6c). The

272 remaining lesions had an intermediate phenotype. PCA revealed that hypoxic lesions are robustly
273 segregated from baseline counterparts (Permanova, Pr(>F)=0.001) (Fig. 6d). Gene Ontology
274 performed for genes overexpressed in hypoxic compared to baseline lesions (FDR>0.01 and
275 FC=1.5 thresholds) revealed statistically significant enrichment for neutrophil chemotaxis and
276 signaling (Supp. Table 5 and Supp. Table 6). Indeed, estimating cell abundances from this
277 unstructured bulk RNA-seq data revealed an increase in neutrophil counts in hypoxic compared
278 to baseline lesions (Fig 6e). The top DEGs between hypoxic compared to baseline lesions
279 included genes associated with neutrophil chemotaxis and survival *CXCL5*, *CXCL8*, *CXCR1*,
280 *CSF3,* and genes encoding for pro-inflammatory cytokines such as *IL1B*, *IL6,* and *OSM* (Fig. 6f
281 and Supp. Table 5). Therefore, our findings in mice are in agreement with the analysis of
282 patient's samples, implicating the presence of neutrophils to the degree of hypoxia in lesions.

283

284 **DISCUSSION**

285

286 Cytolytic CD8 T cells cause severe inflammation in various settings, such as alopecia,
287 malaria, Steven-Johnson syndrome, toxic epidermal necrolysis, cutaneous leishmaniasis, and
288 many others (14, 15, 21, 24, 31–34, 77). However, the factors that promote cytolysis by CD8 T
289 cells in tissue microenvironments are still poorly understood. Here, we show that neutrophils
290 recruited to the skin upon *Leishmania* infection consume oxygen to produce ROS, generating
291 chronic inflammatory hypoxia. The resultant competition for oxygen changes the aerobic
292 microenvironment and promotes the expression of Blimp-1 in recruited CD8 T cells, which
293 results in the expression of the cytolytic molecule granzyme B. Subsequent cell death within the
294 infected area results in tissue damage and chronic neutrophil recruitment (Fig. 6g). Because there

295 are numerous skin diseases associated with cytotoxicity, our findings provide evidence that local
296 inhibition of this pathway should be considered as a strategy to ameliorate these diseases.
297
298 In this regard, preferential expression of cytolytic genes by CD8 T cells in peripheral
299 tissues but not in dLNs is observed in numerous pathogenic conditions. For example, in models
300 of graft-versus-host disease and graft-versus-leukemia, granzyme B is absent in dLNs but present
301 in the skin (9, 11). Additionally, memory CD8 T cells acquire cytolytic activity upon entry into
302 non-lymphoid tissues in vesicular stomatitis virus infections (10). The site-specific function of
303 CD8 T cells is not limited to granzyme B expression. For example, in mice chronically infected
304 with *Trypanosoma cruzi*, CD8 T cells in the spleen produced IFN-γ, while CD8 T cells within
305 the muscle did not (78). Similarly, we found previously that in cutaneous leishmaniasis, CD8 T
306 cells in dLNs produced IFN-γ while CD8 T cells in the skin lacked IFN-γ production (67). Since
307 hypoxic dendritic cells produce less IL-12 (46, 48), this could explain the decrease in CD8 T cell
308 IFN-γ production in lesions (67) and suggests that hypoxia may not only promote pathogenic
309 responses but also prevent protective ones. Conversely, in diseases where cytotoxicity is
310 protective and IFN-γ is pathogenic, the impact of hypoxia would be expected to have the
311 opposite effect. Our confocal microscopy data suggest that hypoxia impacts many other cells
312 beyond CD8 T cells; therefore, it is likely that hypoxia has a much greater role in tissue
313 immunity to *Leishmania*.
314
315 There is substantial clinical and experimental evidence that hypoxia contributes to tumor
316 progression, metastasis, and high mortality (79). While low oxygen levels support myeloid

317 suppressor cell accumulation (80) and tumor cell metastasis (81), hypoxia-inducible factors
318 (HIF) provide CD8 T cells with greater anti-tumor potential (82–84). HIF increases CD8 T cell
319 effector function during chronic viral infections and reduces viral titers but leads to higher
320 mortality (85). These findings agree with the observed increases in perforin expression and
321 killing ability of CD8 T cells cultured in hypoxia (84, 86, 87). Similar results were observed in
322 lupus skin disease, where HIF drove granzyme B expression but, in this case, was independent of
323 hypoxia (88). Hypoxia also alters CD8 T cell metabolism (86) and induces tissue residency (82,
324 89) and exhaustion (90–92) programs. We found a strong correlation between the hypoxic state
325 of CD8 T cells and Blimp-1 expression. Consistent with our findings, hypoxia also triggered
326 Blimp-1 expression in pancreatic tumor cells (81). Since Blimp-1 can instruct tissue residency
327 and exhaustion (62, 93–95), we speculate that hypoxia-driven Blimp-1 expression may also
328 initiate these CD8 T cell programs within cutaneous leishmaniasis lesions, which requires further
329 investigation.

330

331 Another immune cell type implicated in the hypoxia-cytotoxicity axis revealed in our
332 study is neutrophils, which rapidly migrate to infection sites and, in many infections, eliminate
333 invading microbes. However, it is well-recognized that the impact of neutrophils extends beyond
334 pathogen killing, as they also shape the function of other cells within tissues by producing
335 cytokines and chemokines, interacting with dendritic cells and T cells, and consequently
336 affecting disease outcomes. For example, neutrophils producing IL-10 (96) or expressing PD-L1
337 (97) suppress CD4 T cells. Additionally, neutrophils suppress effector responses by tumor-
338 specific T cells in lymph nodes (98) and within tumors (99). In chronic viral infections,
339 suppressive neutrophil subsets reduce the antiviral capabilities of CD8 T cells (100). In contrast,

340 neutrophils facilitate dendritic cell migration to dLNs in contact hypersensitivity and prime
341 allergen-specific CD8 T cells (101). In cutaneous leishmaniasis, neutrophils recruited to lesions
342 can have paradoxical functions depending on the parasite species and mouse model. For
343 example, neutrophils kill *Leishmania* directly by extracellular trap formation or cooperate with
344 macrophages to activate microbicidal activities (102, 103). In contrast, neutrophils reduce
345 costimulatory molecule expression in dendritic cells and silently deliver parasites to
346 macrophages (69, 104, 105). Despite these varied effects, it is clear that chronic recruitment of
347 neutrophils is associated with tissue destruction in cutaneous leishmaniasis (3, 72, 74, 106).
348 Here, we uncovered a new role for neutrophils in cutaneous leishmaniasis lesions by showing
349 that their consumption of oxygen promotes a hypoxic environment, resulting in a phenotypic
350 switch in CD8 T cells.

351

352 Cytotoxic CD8 T cells promote increased inflammation by inducing excessive cell death
353 in lesions and enhancing chronic neutrophil recruitment to the skin (3, 4). In what may be related
354 findings, neutrophil depletion decreases the hypoxic state of herpes stromal keratitis lesions and
355 ameliorates disease (107). In a mouse model of colitis, the respiratory burst by $Gr1^{pos}$ cells -
356 encompassing neutrophils and inflammatory monocytes - induced hypoxia in intestinal epithelial
357 cells, which was critical for disease resolution (108). One limitation of our work is that it does
358 not address the impact of other innate cells and their ability to deplete lesions of oxygen, which
359 could also impact CD8 T cell function. However, our work strongly supports oxygen
360 consumption and neutrophil recruitment as modulators of CD8 T cell granzyme B expression,
361 which fosters the chronic presence of neutrophils in lesions. While the negative impact of this
362 cascade of events is clear in cutaneous leishmaniasis, it could be beneficial in other contexts.

363

364 To be successful, host-directed therapies for infectious diseases should not augment
365 immune responses that damage tissues and must not interfere with responses that control the
366 pathogen (2). Therefore, it is critical to define immune pathways that are pathogenic rather than
367 protective. In cutaneous leishmaniasis, cytotoxicity is an ideal therapeutic target since it
368 associates with treatment failure in patients who receive anti-parasitic drugs (7) and does not
369 control the parasite (3). Patients affected by cutaneous leishmaniasis are frequently treated with
370 anti-parasitic drugs that require intravenous or intramuscular injections every day over the course
371 of 21 days. Because failure rates are high, many patients must go through two and sometimes
372 three rounds of treatment. Our data provide evidence that local inhibition of the cytolytic
373 program can circumvent the use of systemic drugs, which generate considerable side effects, and
374 topical targets should be considered as a new therapeutic strategy for cutaneous leishmaniasis.

375

376 **METHODS**

377

378 **Mice**

379 C57BL/6 CD45.2 and CD45.1 mice (6 weeks old) were purchased from Charles River,
380 and *Prdm1* YFP (here called Blimp-1 reporter), ODD^{cre}/ERT2 (63), Gzmb^{cre}, Blimp-1$^{flox/flox}$, and
381 RAG$^{-/-}$ (B6.12957-RAG1^{tm1Mom}) were purchased from The Jackson Laboratory and crossed in
382 our mouse facility. Cybb$^{-/-}$ mice (109) were obtained from Dr. Juhi Bagaitkar at Nationwide
383 Children's Hospital, Columbus, USA. Experiments assessing Blimp-1 expression with Blimp-1
384 YFP reporter were reproduced using Blimp-1 GFP reporter mice (a kind gift from Stephen Nutt,

385 WEHI, Melbourne, Australia). Gzmb^{cre} mice have the human *GZMB* promoter directing Cre
386 recombinase expression to activated T cells; therefore, it does not directly impact mouse
387 granzyme B expression. Gzmb^{cre} and Blimp-1$^{flox/flox}$ were crossed to generate the deletion of
388 Blimp-1 in activated T cells, and here we called purified CD8 T cells Blimp-1^{cKO}. ODD^{cre}/ERT2
389 and Blimp-1$^{flox/flox}$ were crossed to generate mice in which Blimp-1 deletion was restricted to
390 hypoxic cells in tamoxifen-treated mice. All mice were maintained in a specific pathogen-free
391 environment at The Ohio State University or The University of Pennsylvania Animal Care
392 Facilities.

393

394 **Parasites**

395 *L. major* (strain WHO/MHOM/IL/80/Friedlin) and *L. braziliensis*
396 (MHOM/BR/01/BA788) were grown in Schneider's insect medium (GIBCO) supplemented with
397 20% heat-inactivated FBS (Sigma, St. Louis, MO, USA) and 2 mM glutamine (Thermo-fisher,
398 Waltham, MA, USA). Metacyclic-enriched promastigotes were used for infection (110). Mice
399 were infected with either 10^6 *L. major* or 10^5 *L. braziliensis* intradermally in the ear, and the
400 lesion progression was monitored weekly by measuring the diameter of the ear with a digital
401 caliper.

402

403 **Cell purification and adoptive transfer**

404 Intralesional cell transfer mouse model: CD45.2 and CD45.1 mice were infected with *L.*
405 *major*. CD45.2 mice were euthanized three weeks post-infection, and CD8 T cells from dLNs
406 were purified using a magnetic bead separation kit (Miltenyi Biotec, Germany). 10^6 CD8 T cells

407 were injected into the lesions of CD45.1 mice. Two days post-injection, recipient mice were
408 euthanized, and granzyme B expression in CD8 T cells in the ear and dLN were analyzed by
409 flow cytometry directly ex vivo. $RAG^{-/-}$ mouse model: splenocytes from WT or Blimp-1^{cKO} mice
410 were collected, red blood cells lysed with ACK lysing buffer (LONZA, Switzerland) and CD8 T
411 cells were purified using a magnetic bead separation kit (Miltenyi Biotec, Germany). Three
412 million CD8 T cells were transferred intravenously into $RAG^{-/-}$ mice subsequently infected with
413 *L. braziliensis*. Mice reconstituted with CD8 T cells received four injections of 250 µg of anti-
414 CD4 (clone GK1.5, BioXCell, Lebanon, NH, USA) within the first two weeks.

415

416 **In vivo treatment**

417 FTY720 (Cayman Chemical, Ann Arbor, Michigan, USA) was administered
418 intraperitoneally (3 mg/kg) daily 12 days post-infection and for ten days before euthanasia. To
419 induce Cre expression in the ODD^{cre}/ERT2 mice, tamoxifen (Sigma, St. Louis, MO, USA) was
420 dissolved in corn oil and administered intraperitoneally (67mg/kg) for seven days following
421 infection. Pimonidazole (Hypoxyprobe Inc, Burlington, Massachusetts, USA) was administered
422 intraperitoneally (9 mg/mL, 200 µL) one hour before euthanasia. For neutrophil depletion, mice
423 received injections every three days of 250 µg of anti-Ly6G (clone 1A8, BioXCell, Lebanon,
424 NH, USA) within the first two weeks.

425

426 **Tissue single-cell suspension preparation**

427 Infected ears were harvested, the dorsal and ventral layers of the ear separated, and the
428 ears were incubated in RPMI 1640 (Gibco, Canada) with 250 µg/mL of Liberase TL (Roche

429 Diagnostics, Chicago, IL, USA) for 60-90 mins in a shaker at 37ºC and 5% CO_2. Ears were
430 dissociated using a cell strainer (40 µm, BD Pharmingen, Franklin Lakes, NJ, USA), and an
431 aliquot of the cell suspension was used for parasite titration. dLNs were homogenized using a
432 cell strainer (40 µm, BD Pharmingen, Franklin Lakes, NJ, USA) to obtain single-cell
433 suspensions.

434

435 **Parasite titration**

436 The parasite burden in the ears was quantified as described previously (111). Briefly, the
437 homogenate was serially diluted and incubated at 26°C. The number of viable parasites was
438 calculated from the highest dilution at which parasites were observed after seven days.

439

440 **In vitro stimulation**

441 dLN single-cell suspensions from C57BL/6 infected mice were cultured in 96 well plates
442 "U" bottom with 5µg/mL of plate-bound anti-CD3 (clone 145-2C11, Invitrogen, Waltham, MA,
443 USA), 0.5 µg/mL soluble anti-CD28 (clone 37.51, Invitrogen, Waltham, MA, USA), 37ºC and
444 5% CO_2 for 48 hours in RPMI 1640 containing 100 Units of penicillin and 0.1 mg/mL of
445 Streptomycin (Sigma, St. Louis, MO, USA), 2mM L-Glutamine (Thermo-fisher, Waltham, MA,
446 USA) and 10% FBS (Sigma, St. Louis, MO, USA). Cells were cultured in 1 mM of DMOG
447 (Sigma, St. Louis, MO, USA) dissolved in DMSO or an equivalent volume of DMSO (vehicle)
448 for 48 hours. For mRNA isolation, dLN single-cell suspensions from C57BL/6 infected mice
449 were obtained, and CD8 T cells were purified using a magnetic bead separation kit (Miltenyi
450 Biotec, Germany). CD8 T cells were cultured in 96 well plates "U" bottom with 5µg/mL of

451 plate-bound anti-CD3 (clone 145-2C11, Invitrogen, Waltham, MA, USA), 0.5 μg/mL soluble
452 anti-CD28 (clone 37.51, Invitrogen, Waltham, MA, USA), 20 U/mL recombinant human IL-2 at
453 37ºC and 5% CO_2 for 24 hours in RPMI 1640 (Gibco, Canada) containing 100 Units of penicillin
454 and 0.1 mg/mL of Streptomycin (Sigma, St. Louis, MO, USA), 2mM L-Glutamine (Thermo-
455 fisher, Waltham, MA, USA) and 10% FBS (Sigma, St. Louis, MO, USA). Cells were cultured in
456 1 mM of DMOG (Sigma, St. Louis, MO, USA) dissolved in DMSO or an equivalent volume of
457 DMSO (vehicle).

458

459 **Flow cytometric analysis**

460 Before surface and intracellular staining, cell suspensions were stained with a
461 LIVE/DEAD fixable aqua dead cell stain kit (Thermo-fisher, Waltham, MA, USA), according to
462 manufacturer instructions. Analysis was performed using the FlowJo Software (Tree Star,
463 Ashland, OR, USA), and gates were drawn based on fluorescence minus one control. List of
464 antibodies: CD45 (clone 30-F11), GzmB (clone GB11), CD11b (clone M1/70) (all Invitrogen,
465 Waltham, MA, USA). CD44 (clone IM7, BD Biosciences, Franklin Lakes, NJ, USA), CD45.2
466 (clone 104), CD45.1 (clone A20), CD90 (clone 53-2), CD3 (clone 17A2), CD8β (clone
467 YTS156.7.7), and Ly6G (clone 1A8) (all from BioLegend, San Diego, CA, USA). The stained
468 cells were run on BD FACSymphony A3 or FACSCanto II (BD Biosciences, San Jose, CA,
469 USA).

470

471 **Quantification of *Prdm1* mRNA by qPCR**

472 RNA extraction of in vitro stimulated CD8 T cells was performed using nulceospin RNA,
473 Mini kit (Macherery-Magel, Germany) and used to prepare complementary DNA (cDNA) using
474 iScript Reverse Transcription Supermix for RT-qPCR (Bio-Rad, Hercules, CA, USA) on ABS
475 Proflex Thermal cycler (Thermo-fisher, Waltham, MA, USA). qPCR was carried out on a C1000
476 RT-PCR using iTaq Universal SYBR Green Supermix (all from Bio-Rad, Hercules, CA, USA)
477 and primers targeting *Prdm1* (forward 5'-TTC TCT TGG AAA AAC GTG TGG G-3' and
478 reverse 5'-GGA GCC GGA GCT AGACTT G-3'). The qPCR results were normalized to β-
479 Actin (forward 5'-CGC TGT ATT CCC CTC CAT CG-3' and reverse 5'-CCA GTT GGT AAC
480 AAT GCC ATG T-3'). All reactions were carried out in duplicates, and data is represented as
481 fold-change (FC) over the average expression of vehicle-treated cells.

482

483 **Histology**

484 Two weeks after infection, mice were euthanized, and infected skin (lesions) and
485 contralateral (naïve skin) ears were collected, immediately immersed in 2% paraformaldehyde
486 (PFA) (Thermo-fisher, Waltham, MA, USA), and incubated at room temperature for one hour.
487 Ears were divided in half and re-immersed in PFA for another hour at room temperature.
488 Samples were rinsed and immersed in phosphate-buffered saline (PBS, pH 7.4) (Gibco, Canada)
489 for two hours, followed by cryoprotection in sucrose 30% for 48 hours. Cryoprotected samples
490 were preserved in optimal cutting temperature (OCT) compound (Thermo-fisher, Waltham, MA,
491 USA), and serial sections of 15 µm were obtained on a Tissue-Tek $Cryo_3$ Flex cryostat (Sakura
492 Finetek, Torrance, CA). Sections were collected onto Superfrost Plus microscope slides
493 (Thermo-fisher, Waltham, MA, USA), air-dried, and stored at -80°C.

494

495 **Immunofluorescence, Image acquisition, and Analysis**

496 Slides were dried at room temperature for one hour, rinsed in PBS, and incubated for one
497 hour in blocking solution (4% bovine serum albumin and 0.1% Triton X-100 (both from
498 Thermo-fisher, Waltham, MA, USA) dissolved in PBS). Sections were incubated overnight at
499 4°C with rabbit anti-Pimonidazole antisera (Hypoxyprobe Inc, Burlington, Massachusetts, USA).
500 The slides were washed with PBS and incubated for 4 hours at room temperature with rat anti-
501 mouse Ly6G (cone 1A8, BioLegend, San Diego, CA, USA). Slides were washed with PBS and
502 incubated separately with Alexa Fluor 568 goat anti-rabbit (Invitrogen, Waltham, MA, USA) and
503 Alexa Fluor 488 goat anti-rat (Invitrogen, Waltham, MA, USA). Sections were covered in each
504 secondary antibody for two hours at room temperature. Finally, the sections were counter-stained
505 with the nuclear probe 4',6-diamino-2-phenylindole (DAPI, Biotechne-Tocris, UK). Slides were
506 covered with Prolong™ Gold Antifade Mountant (Invitrogen, Waltham, MA, USA) and kept
507 protected from the light at room temperature for a minimum of 24 hours to allow the mounting
508 media to dry before imaging. Representative images were acquired with 10x and 20x objectives
509 in an Olympus FV3000 confocal microscopy (Olympus Corporation, Japan). The color of the
510 different structures was digitally inverted to better match the presented data in this manuscript.
511 Using ImageJ software (version 1.53, National Institute of Health), 27 regions of interest (ROIs)
512 measuring 600x40 µm were created. From the low signal edge to the other, the pixel intensity
513 values of each ROI were obtained.

514

515 **Transcriptional profiling of purified mouse CD8 T cells**

516 C57BL/6 mice were infected with *L. major,* and five weeks post-infection, mice were
517 euthanized; cells from the infected ear and dLN cells were purified and stained for flow

518 cytometric analysis. Antigen-experienced CD8 T cells were purified using FACSAria cell sorter
519 (gating strategy: live, singlets, $CD90^{+}$, $CD8^{+}CD44^{high}$), and RNA was extracted using the
520 RNeasy Plus Mini Kit (QIAGEN, Germany) according to the manufacturer's instructions and
521 used to prepare Poly(A)+-enriched cDNA libraries Illumina TruSeq Stranded mRNA library
522 prep workflow. Ribo-Zero Gold rRNA depletion (Illumina, San Diego, CA, USA) removed
523 ribosomal content. Quality assessment and quantification of RNA preparations and libraries were
524 performed using an Agilent 4200 TapeStation and Qubit 3, respectively. Samples were
525 sequenced on an Illumina NextSeq 500 to produce 75–base pair single-end reads. The raw reads
526 were mapped to the mouse reference transcriptome (Ensembl; Mus musculus version 108) using
527 Kallisto version 0.46.0, and MultiQC v1.9 was used to check the quality of the alignment.

528 All subsequent analyses were conducted using the statistical computing environment R
529 version 4.1.0, RStudio version 1.4.1717, and Bioconductor version 3.13. Briefly, transcript
530 quantification data were summarized to genes using the BiomaRt and tximport package and
531 normalized using the trimmed mean of M values (TMM) method in edgeR. Genes with <1 CPM
532 in at least three samples were filtered out. Normalized filtered data were variance-stabilized
533 using the voom function in limma, and Differential Gene Expression analysis was performed
534 with linear modeling using limma after correcting for multiple testing using Benjamini-Hochberg
535 FDR correction. The list of 7 genes encoding for transcription factors associated with effector
536 like T cell functions was gathered from (55–57). Hypoxic enrichment per RNA-seq sample was
537 calculate with single-sample GSEA using the GSVA R package. The 5 Hypoxia-related
538 signatures used to estimate those levels were downloaded from: Harris et al. 2022 (58), Hallmark
539 systematic name (sn) #M5891, Biocarta sn #M13324, Biocarta sn #M14863 and Reactome sn
540 #M641.

541

542 **Hypoxia-related transcriptional analyses on lesion biopsies from cutaneous leishmaniasis**
543 **patients**

544 Data in Fig. 6 are derived from published transcriptional profiling (51, 76). The analysis
545 carried out for this current study was performed from the filtered, normalized gene expression
546 matrix available for download as a text file on NCBI GEO accession #GSE162760 and
547 #GSE214397. All subsequent analyses were conducted similarly to the purified mouse CD8 T
548 cells RNA-seq dataset. Hypoxia scores for the human RNA-seq dataset were calculated using the
549 Harris et al. gene signature (58). Unsupervised hierarchical clustering classifying lesion samples
550 according to their "hypoxic scores" was performed with maximum distances and Ward's D2
551 minimum variance. Permanova statistical testing was performed with the vegan R package. Gene
552 Set Enrichment Analysis (GSEA) was performed using the Broad Institute software version
553 4.3.2. Gene Ontology (GO) analyses were carried out using DAVID Bioinformatics Resources
554 (2021 Update) from NIAID/NIH and biological process terms, clustering genesets by annotation
555 similarity. MCP-counter and immundeconv R packages were combined to estimate neutrophil
556 abundances from the unstructured RNA-seq dataset. Data visualization was mostly performed in
557 GraphPad Prism version 10 and in R programming language using tidyverse and gplots tools.

558

559 **Statistics**

560 Statistical significance was determined using the two-tailed unpaired Student's *t*-test. The
561 specific transcriptional analysis section describes detailed statistical analysis for RNA

562 sequencing. Differences were considered significant when $p \leq 0.05$ (*), $p \leq 0.01$ (**), $p \leq 0.001$
563 (***), or $p \leq 0.0001$ (****).

564 **Study Approval**

565 This study was carried out per the recommendations in the Guide for the Care and Use of
566 Laboratory Animals of the National Institutes of Health. The Institutional Animal Care and Use
567 Committee, The Ohio State University, and The University of Pennsylvania approved the
568 protocol.

569

570 **Data availability**

571 Raw sequence data from purified mouse CD8 T cells are available on the NCBI GEO
572 BioProject PRJNA794119. The complete RNA-seq data analysis, R code, file inputs, and outputs
573 used to perform the transcriptional analysis presented in this current manuscript are available on
574 the GitHub repository "Hypoxia_FON" (https://github.com/camilafarias112/Hypoxia_FON).

575

576 **Author contributions**

577 EAF, CFA, RAS, EDSH, KM, LAS, WZ, CIO, GDW, PLC, and FON designed research
578 studies; EAF, CFA, RAS, EDSH, KM, LAS, WZ, FON, and PLC conducted experiments;
579 EAF, CFA, KAM, WZ, and FON analyzed and interpreted the data; EAF, CFA, and FON wrote
580 the manuscript. FON supervised the study.

581

582 **Acknowledgments**

583 This work was supported by National Institutes of Health grant R01AI162711 (FON) ,
584 National Institute of Health training program T32 AI165391 “Interdisciplinary Program in
585 Microbe-Host Biology” (EAF), National Institute of Health training program T32 AI118684
586 (WZ), Host-Microbial Analytic and Repository Core in the Center for Molecular Studies in
587 Digestive and Liver Diseases (P30DK050306) (GDW). The authors would like to thank Dr. Juhi
588 Bagaitkar for providing Cybb$^{-/-}$ mice.

589

590 **Supplemental Material**

591 Supplemental Figure 1. Genes overexpressed in CD8 T cells purified from dLNs compared to
592 lesions.

593 Supplemental Figure 2. Pimonidazole expression in Leishmania-infected skin.

594 Supplemental Figure 3. Neutrophil and pimonidazole expression in Leishmania-infected skin.

595 Supplemental Table 1. Differentially expressed genes between CD8 T cells isolated from the
596 lesions compared to the dLN.

597 Supplemental Table 2. Gene Set Enrichment Analysis (GSEA) between CD8 T cells isolated
598 from the lesions compared to the dLN accessing the C2 CP collection of pathways.

599 Supplemental Table 3. Clinical metadata from lesions of patients with cutaneous leishmaniasis,
600 including the associated Harris et al. Hypoxia scores and Neutrophil abundances.

601 Supplemental Table 4. Clinical metadata from blood of patients with cutaneous leishmaniasis,
602 including the associated Harris et al. Hypoxia scores.

603 Supplemental Table 5. Differentially expressed genes between hypoxic and baseline lesions from
604 patients with cutaneous leishmaniasis.

605 Supplemental Table 6. Gene Ontology (GO) performed on DEGs between hypoxic and baseline
606 lesions from patients with cutaneous leishmaniasis accessing the Biological Process database.

607 **References**

608

609 1. Scott P, Novais FO. Cutaneous leishmaniasis: immune responses in protection and pathogenesis.. *Nat. Rev.*
610 *Immunol.* 2016;16(9):581–592.
611 2. Novais FO, Amorim CF, Scott P. Host-Directed Therapies for Cutaneous Leishmaniasis.. *Front. Immunol.*
612 2021;12:660183.
613 3. Novais FO et al. Cytotoxic T cells mediate pathology and metastasis in cutaneous leishmaniasis.. *PLoS Pathog.*
614 2013;9(7):e1003504.
615 4. Novais FO et al. CD8+ T cell cytotoxicity mediates pathology in the skin by inflammasome activation and IL-1β
616 production.. *PLoS Pathog.* 2017;13(2):e1006196.
617 5. Novais FO, Scott P. CD8+ T cells in cutaneous leishmaniasis: the good, the bad, and the ugly.. *Semin*
618 *Immunopathol* 2015;37(3):251–259.
619 6. Crosby EJ, Clark M, Novais FO, Wherry EJ, Scott P. Lymphocytic Choriomeningitis Virus Expands a Population
620 of NKG2D+CD8+ T Cells That Exacerbates Disease in Mice Coinfected with Leishmania major.. *J. Immunol.*
621 2015;195(7):3301–3310.
622 7. Amorim CF et al. Variable gene expression and parasite load predict treatment outcome in cutaneous
623 leishmaniasis.. *Sci. Transl. Med.* 2019;11(519). doi:10.1126/scitranslmed.aax4204
624 8. Silverio JC et al. CD8+ T-cells expressing interferon gamma or perforin play antagonistic roles in heart injury in
625 experimental Trypanosoma cruzi-elicited cardiomyopathy.. *PLoS Pathog.* 2012;8(4):e1002645.
626 9. Santos E Sousa P et al. Peripheral tissues reprogram CD8+ T cells for pathogenicity during graft-versus-host
627 disease.. *JCI Insight* 2018;3(5). doi:10.1172/jci.insight.97011
628 10. Marzo AL, Yagita H, Lefrançois L. Cutting edge: migration to nonlymphoid tissues results in functional
629 conversion of central to effector memory CD8 T cells.. *J. Immunol.* 2007;179(1):36–40.
630 11. Michonneau D et al. The PD-1 Axis Enforces an Anatomical Segregation of CTL Activity that Creates Tumor
631 Niches after Allogeneic Hematopoietic Stem Cell Transplantation.. *Immunity* 2016;44(1):143–154.
632 12. Weisberg SP, Ural BB, Farber DL. Tissue-specific immunity for a changing world.. *Cell* 2021;184(6):1517–
633 1529.
634 13. Schenkel JM, Pauken KE. Localization, tissue biology and T cell state - implications for cancer immunotherapy..
635 *Nat. Rev. Immunol.* [published online ahead of print: May 30, 2023]; doi:10.1038/s41577-023-00884-8
636 14. Ammar M et al. Involvement of granzyme B and granulysin in the cytotoxic response in lichen planus.. *J. Cutan.*
637 *Pathol.* 2008;35(7):630–634.
638 15. Hiroyasu S et al. Granzyme B inhibition reduces disease severity in autoimmune blistering diseases.. *Nat.*
639 *Commun.* 2021;12(1):302.
640 16. Kaminski L-C et al. Cytotoxic T Cell-Derived Granzyme B Is Increased in Severe Plasmodium Falciparum
641 Malaria.. *Front. Immunol.* 2019;10:2917.
642 17. Voskoboinik I, Whisstock JC, Trapani JA. Perforin and granzymes: function, dysfunction and human pathology..
643 *Nat. Rev. Immunol.* 2015;15(6):388–400.
644 18. Walch M et al. Cytotoxic cells kill intracellular bacteria through granulysin-mediated delivery of granzymes..
645 *Cell* 2014;157(6):1309–1323.
646 19. Eeka P, Phanithi PB. Cytotoxic T Lymphocyte Granzyme-b mediates neuronal cell death during Plasmodium
647 berghei ANKA induced experimental cerebral malaria.. *Neurosci. Lett.* 2018;664:58–65.
648 20. Ji N-N et al. CTL-Derived Granzyme B Participates in Hippocampal Neuronal Apoptosis Induced by Cardiac
649 Arrest and Resuscitation in Rats.. *Front. Neurol.* 2019;10:1306.
650 21. Gleave A, Granville DJ. Granzyme B in autoimmune skin disease.. *Biomolecules* 2023;13(2).
651 doi:10.3390/biom13020388
652 22. Dotiwala F et al. Killer lymphocytes use granulysin, perforin and granzymes to kill intracellular parasites.. *Nat.*
653 *Med.* 2016;22(2):210–216.
654 23. Metkar SS et al. Human and mouse granzyme A induce a proinflammatory cytokine response.. *Immunity*
655 2008;29(5):720–733.
656 24. Shen Y et al. Topical small molecule granzyme B inhibitor improves remodeling in a murine model of impaired
657 burn wound healing.. *Exp Mol Med* 2018;50(5):1–11.
658 25. Park S et al. Granzyme A–producing T helper cells are critical for acute graft-versus-host disease. *JCI Insight*
659 2020;
660 26. Parasa VR et al. Enhanced CD8+ cytolytic T cell responses in the peripheral circulation of patients with

661 sarcoidosis and non-Löfgren's disease.. *Respir. Med.* 2018;138S:S38–S44.
662 27. Junqueira C et al. Cytotoxic CD8+ T cells recognize and kill Plasmodium vivax-infected reticulocytes.. *Nat.*
663 *Med.* 2018;24(9):1330–1336.
664 28. Balin SJ et al. Human antimicrobial cytotoxic T lymphocytes, defined by NK receptors and antimicrobial
665 proteins, kill intracellular bacteria.. *Sci. Immunol.* 2018;3(26). doi:10.1126/sciimmunol.aat7668
666 29. Trivedi P et al. Perforin facilitates beta cell killing and regulates autoreactive CD8+ T-cell responses to antigen
667 in mouse models of type 1 diabetes.. *Immunol. Cell Biol.* 2016;94(4):334–341.
668 30. Vičić M et al. Cytotoxic T lymphocytes as a potential brake of keratinocyte proliferation in psoriasis.. *Med.*
669 *Hypotheses* 2016;87:66–68.
670 31. Patra V et al. Accumulation of Cytotoxic Skin Resident Memory T Cells and Increased Expression of IL-15 in
671 Lesional Skin of Polymorphic Light Eruption.. *Front Med (Lausanne)* 2022;9:908047.
672 32. Chung W-H et al. Granulysin is a key mediator for disseminated keratinocyte death in Stevens-Johnson
673 syndrome and toxic epidermal necrolysis.. *Nat. Med.* 2008;14(12):1343–1350.
674 33. Haque A et al. Granzyme B expression by CD8+ T cells is required for the development of experimental
675 cerebral malaria.. *J. Immunol.* 2011;186(11):6148–6156.
676 34. Xing L et al. Alopecia areata is driven by cytotoxic T lymphocytes and is reversed by JAK inhibition.. *Nat. Med.*
677 2014;20(9):1043–1049.
678 35. Zloza A et al. Engagement of NK receptor NKG2D, but not 2B4, results in self-reactive CD8+ T cells and
679 autoimmune vitiligo.. *Autoimmunity* 2011;44(8):599–606.
680 36. Jacquemin C et al. NKG2D Defines a Subset of Skin Effector Memory CD8 T Cells with Proinflammatory
681 Functions in Vitiligo.. *J. Invest. Dermatol.* 2020;140(6):1143–1153.e5.
682 37. van den Boorn JG et al. Autoimmune destruction of skin melanocytes by perilesional T cells from vitiligo
683 patients.. *J. Invest. Dermatol.* 2009;129(9):2220–2232.
684 38. Taylor CT, Scholz CC. The effect of HIF on metabolism and immunity.. *Nat. Rev. Nephrol.* 2022;18(9):573–
685 587.
686 39. Schatz V, Neubert P, Rieger F, Jantsch J. Hypoxia, Hypoxia-Inducible Factor-1α, and Innate Antileishmanial
687 Immune Responses.. *Front. Immunol.* 2018;9:216.
688 40. Charpentier T, Hammami A, Stäger S. Hypoxia inducible factor 1α: A critical factor for the immune response to
689 pathogens and Leishmania.. *Cell Immunol.* 2016;309:42–49.
690 41. Mahnke A et al. Hypoxia in Leishmania major skin lesions impairs the NO-dependent leishmanicidal activity of
691 macrophages.. *J. Invest. Dermatol.* 2014;134(9):2339–2346.
692 42. Bowlin A et al. Hypoxia inducible factor signaling in macrophages promotes lymphangiogenesis in Leishmania
693 major infection.. *Infect. Immun.* [published online ahead of print: May 24, 2021]; doi:10.1128/IAI.00124-21
694 43. Degrossoli A, Colhone MC, Arrais-Silva WW, Giorgio S. Hypoxia modulates expression of the 70-kD heat
695 shock protein and reduces Leishmania infection in macrophages.. *J Biomed Sci* 2004;11(6):847–854.
696 44. Colhone MC, Arrais-Silva WW, Picoli C, Giorgio S. Effect of hypoxia on macrophage infection by Leishmania
697 amazonensis.. *J. Parasitol.* 2004;90(3):510–515.
698 45. Arrais-Silva WW, Paffaro VA, Yamada AT, Giorgio S. Expression of hypoxia-inducible factor-1alpha in the
699 cutaneous lesions of BALB/c mice infected with Leishmania amazonensis.. *Exp Mol Pathol* 2005;78(1):49–54.
700 46. Hammami A, Abidin BM, Heinonen KM, Stäger S. HIF-1α hampers dendritic cell function and Th1 generation
701 during chronic visceral leishmaniasis.. *Sci. Rep.* 2018;8(1):3500.
702 47. Hammami A et al. HIF-1α is a key regulator in potentiating suppressor activity and limiting the microbicidal
703 capacity of MDSC-like cells during visceral leishmaniasis.. *PLoS Pathog.* 2017;13(9):e1006616.
704 48. Hammami A, Charpentier T, Smans M, Stäger S. IRF-5-Mediated Inflammation Limits CD8+ T Cell Expansion
705 by Inducing HIF-1α and Impairing Dendritic Cell Functions during Leishmania Infection.. *PLoS Pathog.*
706 2015;11(6):e1004938.
707 49. Mesquita I et al. The Absence of HIF-1α Increases Susceptibility to Leishmania donovani Infection via
708 Activation of BNIP3/mTOR/SREBP-1c Axis.. *Cell Rep.* 2020;30(12):4052–4064.e7.
709 50. Novais FO, Nguyen BT, Scott P. Granzyme B inhibition by tofacitinib blocks the pathology induced by CD8 T
710 cells in cutaneous leishmaniasis.. *J. Invest. Dermatol.* 2021;141(3):575–585.
711 51. Farias Amorim C et al. The skin microbiome enhances disease through IL-1b and delays healing in cutaneous
712 leishmaniasis patients.. *medRxiv* [published online ahead of print: February 6, 2023];
713 doi:10.1101/2023.02.02.23285247
714 52. Novais FO et al. Genomic profiling of human Leishmania braziliensis lesions identifies transcriptional modules
715 associated with cutaneous immunopathology.. *J. Invest. Dermatol.* 2015;135(1):94–101.
716 53. Crosby EJ, Goldschmidt MH, Wherry EJ, Scott P. Engagement of NKG2D on bystander memory CD8 T cells

717 promotes increased immunopathology following Leishmania major infection.. *PLoS Pathog.* 2014;10(2):e1003970.
718 54. Santos C da S et al. CD8(+) granzyme B(+)-mediated tissue injury vs. CD4(+)IFNγ(+)-mediated parasite killing
719 in human cutaneous leishmaniasis.. *J. Invest. Dermatol.* 2013;133(6):1533–1540.
720 55. Chen Y, Zander R, Khatun A, Schauder DM, Cui W. Transcriptional and epigenetic regulation of effector and
721 memory CD8 T cell differentiation.. *Front. Immunol.* 2018;9:2826.
722 56. Chang JT, Wherry EJ, Goldrath AW. Molecular regulation of effector and memory T cell differentiation.. *Nat.*
723 *Immunol.* 2014;15(12):1104–1115.
724 57. Yu B et al. Epigenetic landscapes reveal transcription factors that regulate CD8+ T cell differentiation.. *Nat.*
725 *Immunol.* 2017;18(5):573–582.
726 58. Harris AL. Hypoxia--a key regulatory factor in tumour growth.. *Nat. Rev. Cancer* 2002;2(1):38–47.
727 59. Evans SM, Schrlau AE, Chalian AA, Zhang P, Koch CJ. Oxygen levels in normal and previously irradiated
728 human skin as assessed by EF5 binding.. *J. Invest. Dermatol.* 2006;126(12):2596–2606.
729 60. Evans NTS, Naylor PFD. The systemic oxygen supply to the surface of human skin. *Respir Physiol*
730 1967;3(1):21–37.
731 61. Friedman ES et al. Microbes vs. chemistry in the origin of the anaerobic gut lumen.. *Proc. Natl. Acad. Sci. USA*
732 2018;115(16):4170–4175.
733 62. Shin H et al. A role for the transcriptional repressor Blimp-1 in CD8(+) T cell exhaustion during chronic viral
734 infection.. *Immunity* 2009;31(2):309–320.
735 63. Lin Q, Huang Y, Giordano FJ, Yun Z. Generation of a hypoxia-sensing mouse model.. *Genesis* 2020;58(3–
736 4):e23352.
737 64. Fu S-H, Yeh L-T, Chu C-C, Yen BL-J, Sytwu H-K. New insights into Blimp-1 in T lymphocytes: a divergent
738 regulator of cell destiny and effector function.. *J Biomed Sci* 2017;24(1):49.
739 65. Montes de Oca M et al. Blimp-1-Dependent IL-10 Production by Tr1 Cells Regulates TNF-Mediated Tissue
740 Pathology.. *PLoS Pathog.* 2016;12(1):e1005398.
741 66. Belkaid Y et al. CD8+ T cells are required for primary immunity in C57BL/6 mice following low-dose,
742 intradermal challenge with Leishmania major.. *J. Immunol.* 2002;168(8):3992–4000.
743 67. Novais FO, Wong AC, Villareal DO, Beiting DP, Scott P. CD8+ T Cells Lack Local Signals To Produce IFN-γ
744 in the Skin during Leishmania Infection.. *J. Immunol.* 2018;200(5):1737–1745.
745 68. Weinkopff T, Roys H, Bowlin A, Scott P. Leishmania Infection Induces Macrophage Vascular Endothelial
746 Growth Factor A Production in an ARNT/HIF-Dependent Manner.. *Infect. Immun.* 2019;87(11).
747 doi:10.1128/IAI.00088-19
748 69. Peters NC et al. In vivo imaging reveals an essential role for neutrophils in leishmaniasis transmitted by sand
749 flies.. *Science* 2008;321(5891):970–974.
750 70. Passelli K, Billion O, Tacchini-Cottier F. The impact of neutrophil recruitment to the skin on the pathology
751 induced by leishmania infection.. *Front. Immunol.* 2021;12:649348.
752 71. Pedraza-Zamora CP, Delgado-Domínguez J, Zamora-Chimal J, Becker I. Th17 cells and neutrophils: Close
753 collaborators in chronic Leishmania mexicana infections leading to disease severity.. *Parasite Immunol* 2017;39(4).
754 doi:10.1111/pim.12420
755 72. Charmoy M et al. The Nlrp3 inflammasome, IL-1β, and neutrophil recruitment are required for susceptibility to
756 a nonhealing strain of Leishmania major in C57BL/6 mice.. *Eur. J. Immunol.* 2016;46(4):897–911.
757 73. Gonçalves-de-Albuquerque S da C et al. The equivocal role of th17 cells and neutrophils on
758 immunopathogenesis of leishmaniasis.. *Front. Immunol.* 2017;8:1437.
759 74. Gimblet C et al. Cutaneous Leishmaniasis Induces a Transmissible Dysbiotic Skin Microbiota that Promotes
760 Skin Inflammation.. *Cell Host Microbe* 2017;22(1):13–24.e4.
761 75. Moghadam ZM, Henneke P, Kolter J. From flies to men: ROS and the NADPH oxidase in phagocytes.. *Front.*
762 *Cell Dev. Biol.* 2021;9:628991.
763 76. Farias Amorim C et al. Localized skin inflammation during cutaneous leishmaniasis drives a chronic, systemic
764 IFN-γ signature.. *PLoS Negl. Trop. Dis.* 2021;15(4):e0009321.
765 77. Turner CT et al. Granzyme B Contributes to Barrier Dysfunction in Oxazolone-Induced Skin Inflammation
766 through E-Cadherin and FLG Cleavage.. *J. Invest. Dermatol.* 2021;141(1):36–47.
767 78. Leavey JK, Tarleton RL. Cutting edge: dysfunctional CD8+ T cells reside in nonlymphoid tissues during chronic
768 Trypanosoma cruzi infection.. *J. Immunol.* 2003;170(5):2264–2268.
769 79. Chouaib S, Noman MZ, Kosmatopoulos K, Curran MA. Hypoxic stress: obstacles and opportunities for
770 innovative immunotherapy of cancer.. *Oncogene* 2017;36(4):439–445.
771 80. Chiu DK-C et al. Hypoxia inducible factor HIF-1 promotes myeloid-derived suppressor cells accumulation
772 through ENTPD2/CD39L1 in hepatocellular carcinoma.. *Nat. Commun.* 2017;8(1):517.

773 81. Chiou S-H et al. BLIMP1 induces transient metastatic heterogeneity in pancreatic cancer.. *Cancer Discov.*
774 2017;7(10):1184–1199.
775 82. Liikanen I et al. Hypoxia-inducible factor activity promotes antitumor effector function and tissue residency by
776 CD8+ T cells.. *J. Clin. Invest.* 2021;131(7). doi:10.1172/JCI143729
777 83. Veliça P et al. Modified Hypoxia-Inducible Factor Expression in CD8+ T Cells Increases Antitumor Efficacy..
778 *Cancer Immunol Res* 2021;9(4):401–414.
779 84. Cunha PP et al. Oxygen levels at the time of activation determine T cell persistence and immunotherapeutic
780 efficacy.. *Elife* 2023;12. doi:10.7554/eLife.84280
781 85. Doedens AL et al. Hypoxia-inducible factors enhance the effector responses of CD8(+) T cells to persistent
782 antigen.. *Nat. Immunol.* 2013;14(11):1173–1182.
783 86. Finlay DK et al. PDK1 regulation of mTOR and hypoxia-inducible factor 1 integrate metabolism and migration
784 of CD8+ T cells.. *J. Exp. Med.* 2012;209(13):2441–2453.
785 87. Gropper Y et al. Culturing CTLs under Hypoxic Conditions Enhances Their Cytolysis and Improves Their Anti-
786 tumor Function.. *Cell Rep.* 2017;20(11):2547–2555.
787 88. Little AJ et al. HIF-1 regulates pathogenic cytotoxic T cells in lupus skin disease. *JCI Insight* 2023;
788 89. Hasan F, Chiu Y, Shaw RM, Wang J, Yee C. Hypoxia acts as an environmental cue for the human tissue-
789 resident memory T cell differentiation program.. *JCI Insight* 2021;6(10). doi:10.1172/jci.insight.138970
790 90. Bannoud N et al. Hypoxia supports differentiation of terminally exhausted CD8 T cells.. *Front. Immunol.*
791 2021;12:660944.
792 91. Scharping NE et al. Mitochondrial stress induced by continuous stimulation under hypoxia rapidly drives T cell
793 exhaustion.. *Nat. Immunol.* 2021;22(2):205–215.
794 92. Ford BR et al. Altered costimulatory signals and hypoxia support chromatin landscapes limiting the functional
795 potential of exhausted T cells in cancer. *BioRxiv* [published online ahead of print: July 12, 2021];
796 doi:10.1101/2021.07.11.451947
797 93. Behr FM et al. Blimp-1 Rather Than Hobit Drives the Formation of Tissue-Resident Memory CD8+ T Cells in
798 the Lungs.. *Front. Immunol.* 2019;10:400.
799 94. Mackay LK et al. Hobit and Blimp1 instruct a universal transcriptional program of tissue residency in
800 lymphocytes.. *Science* 2016;352(6284):459–463.
801 95. Kragten NAM et al. Blimp-1 induces and Hobit maintains the cytotoxic mediator granzyme B in CD8 T cells..
802 *Eur. J. Immunol.* 2018;48(10):1644–1662.
803 96. Doz E, Lombard R, Carreras F, Buzoni-Gatel D, Winter N. Mycobacteria-infected dendritic cells attract
804 neutrophils that produce IL-10 and specifically shut down Th17 CD4 T cells through their IL-10 receptor.. *J.*
805 *Immunol.* 2013;191(7):3818–3826.
806 97. Rambault M et al. Neutrophils encompass a regulatory subset suppressing T cells in apparently healthy cattle
807 and mice.. *Front. Immunol.* 2021;12:625244.
808 98. Glodde N et al. Reactive Neutrophil Responses Dependent on the Receptor Tyrosine Kinase c-MET Limit
809 Cancer Immunotherapy.. *Immunity* 2017;47(4):789–802.e9.
810 99. Coffelt SB et al. IL-17-producing γδ T cells and neutrophils conspire to promote breast cancer metastasis..
811 *Nature* 2015;522(7556):345–348.
812 100. Volberding PJ et al. Suppressive neutrophils require PIM1 for metabolic fitness and survival during chronic
813 viral infection.. *Cell Rep.* 2021;35(8):109160.
814 101. Weber FC et al. Neutrophils are required for both the sensitization and elicitation phase of contact
815 hypersensitivity.. *J. Exp. Med.* 2015;212(1):15–22.
816 102. Novais FO et al. Neutrophils and macrophages cooperate in host resistance against Leishmania braziliensis
817 infection.. *J. Immunol.* 2009;183(12):8088–8098.
818 103. Guimarães-Costa AB et al. Leishmania amazonensis promastigotes induce and are killed by neutrophil
819 extracellular traps.. *Proc. Natl. Acad. Sci. USA* 2009;106(16):6748–6753.
820 104. Ribeiro-Gomes FL, Peters NC, Debrabant A, Sacks DL. Efficient capture of infected neutrophils by dendritic
821 cells in the skin inhibits the early anti-leishmania response.. *PLoS Pathog.* 2012;8(2):e1002536.
822 105. van Zandbergen G et al. Cutting edge: neutrophil granulocyte serves as a vector for Leishmania entry into
823 macrophages.. *J. Immunol.* 2004;173(11):6521–6525.
824 106. Gonzalez-Lombana C et al. IL-17 mediates immunopathology in the absence of IL-10 following Leishmania
825 major infection.. *PLoS Pathog.* 2013;9(3):e1003243.
826 107. Rao P, Suvas S. Development of inflammatory hypoxia and prevalence of glycolytic metabolism in progressing
827 herpes stromal keratitis lesions.. *J. Immunol.* 2019;202(2):514–526.
828 108. Campbell EL et al. Transmigrating neutrophils shape the mucosal microenvironment through localized oxygen

829 depletion to influence resolution of inflammation.. *Immunity* 2014;40(1):66–77.
830 109. Pollock JD et al. Mouse model of X-linked chronic granulomatous disease, an inherited defect in phagocyte
831 superoxide production.. *Nat. Genet.* 1995;9(2):202–209.
832 110. Späth GF, Beverley SM. A lipophosphoglycan-independent method for isolation of infective Leishmania
833 metacyclic promastigotes by density gradient centrifugation.. *Exp Parasitol* 2001;99(2):97–103.
834 111. Uzonna JE, Joyce KL, Scott P. Low dose Leishmania major promotes a transient T helper cell type 2 response
835 that is down-regulated by interferon gamma-producing CD8+ T cells.. *J. Exp. Med.* 2004;199(11):1559–1566.
836
837
838

Figure 1

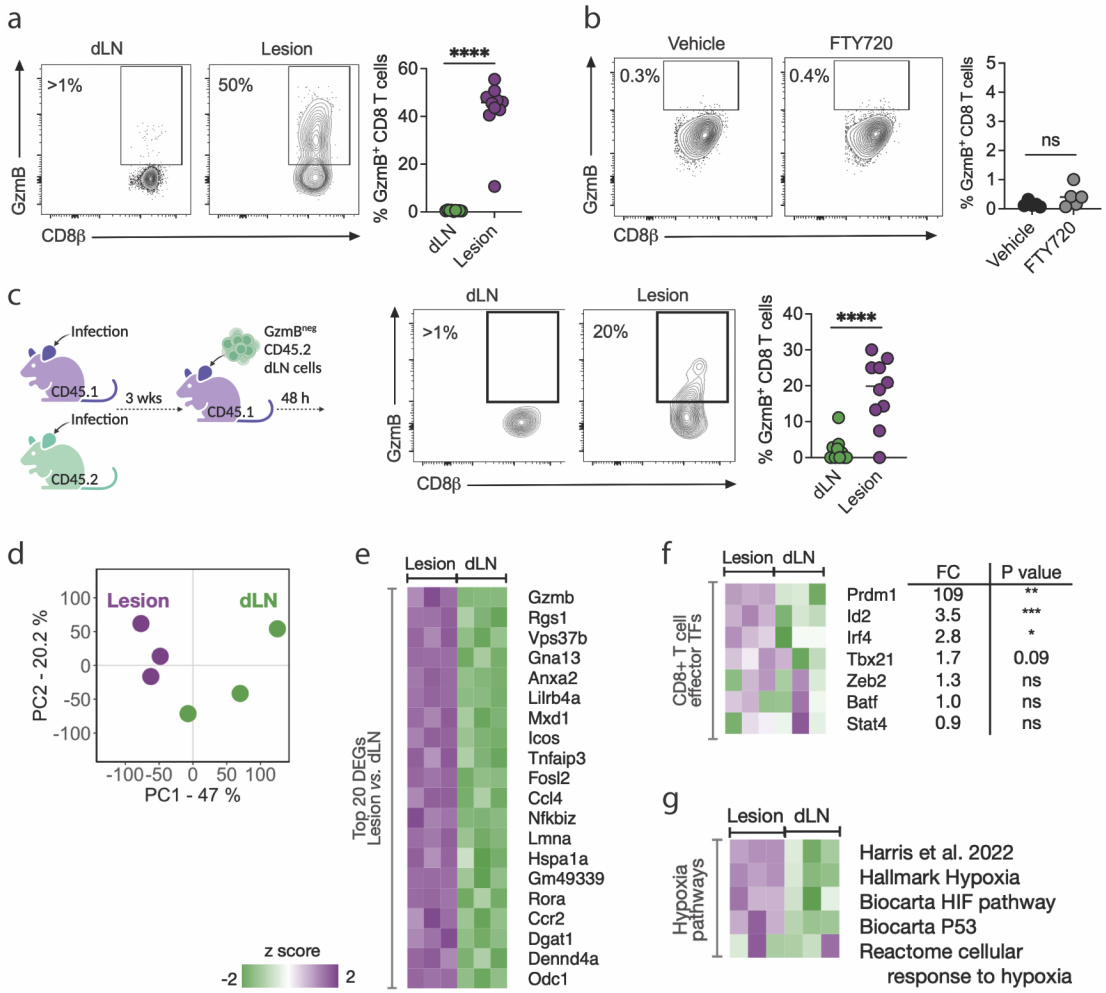

Fig 1. CD8 T cell function is tissue-specific.

(a) Granzyme B (GzmB) expression in CD8 T cells from dLNs and lesions from C57BL/6 mice in week two post-infection with *L. major*. Representative data from more than three experiments with at least four mice per experiment. (b) Granzyme B expression in dLN CD8 T cells from *L. major* infected C57BL/6 mice treated with FTY720 or vehicle daily 12 days post-infection for 10 days. Data from one independent experiment with five mice per group. (c - left) Schematic representation of the transfer of CD45.2 dLN purified CD8 T cells into the lesions of CD45.1 recipients, both infected for three weeks. (c - right) Granzyme B expression in donor CD8 T cells from dLNs and lesions from recipient mice 48 hours post-transfer. Data from 2 experiments independent experiments combined. (d-g) RNA-seq analyses from antigen-experienced ($CD44^{high}$) CD8 T cells purified from dLNs and lesions of *L. major*-infected mice in week five. (d) Principal component analysis showing principal component 1 (PC1) and PC2. (e) Heat map of top 20 differentially expressed genes (DEGs) between purified CD8 T cells from the lesions compared to dLN (FDR>0.05 and FC=1.5). (f) Expression of genes encoding for transcription factors associated with effector-like T cell functions is represented in a heat map, as well as fold-change (FC) between lesional and dLN CD8 T cells. (g) Heatmap of hypoxia-related pathways enriched in lesional and dLN CD8 T cells. *P ≤ 0.05, **P ≤ 0.01, ***P ≤ 0.001 and ****P ≤ 0.0001. ns = non-significant. FDR = false discovery rates. FC = fold change.

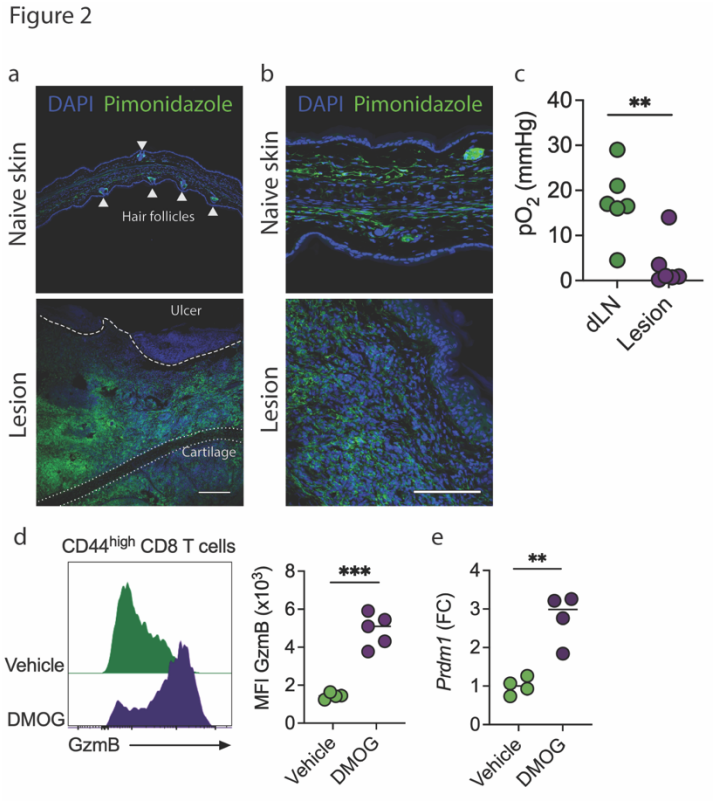

Fig 2. Hypoxia induces granzyme B and *Prdm1* expression in CD8 T cells.

(a-b) Immunofluorescence staining and confocal microscopy of horizontal sections from lesions of *L. major* C57BL/6-infected mice for two weeks. Mice received pimonidazole one hour before euthanasia. The top panels show contralateral ears (naïve skin), and the bottom panels are from infected ears (lesions). Pimonidazole (green) and nuclear stain DAPI (blue). Representative image from two naïve and three infected ears. Bars (a) 200 µm and (b) 100 µm. (c) Partial pressure of oxygen in mmHg in dLNs and lesions of C57BL/6 mice infected with *L. major* for two weeks. Data from two independent experiments combined. (d) Granzyme B (GzmB) expression in CD8 T cells from dLNs of C57BL/6 mice infected with *L. major* cultured with Dimethyloxalylglycine (DMOG) or vehicle. (e) Fold-change (FC) of *Prdm1* mRNA over the average expression of vehicle-treated cells measured by qPCR in DMOG or vehicle-treated purified CD8 T cells. **$P \leq 0.01$ and ***$P \leq 0.001$

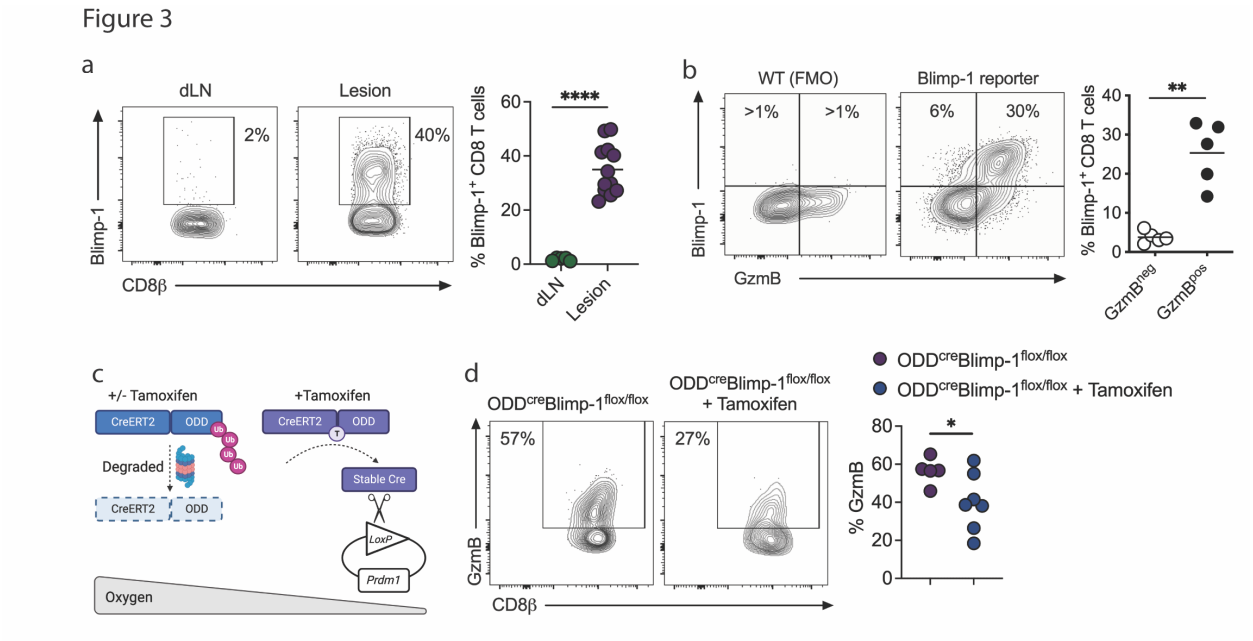

Fig 3. Blimp-1 expression is induced by hypoxia within skin lesions.

(a) Blimp-1 YFP reporter mice expression in CD8 T cells from dLNs and lesions from Blimp-1 reporter mice infected with *L. major* for one week. Data from two independent experiments combined. (b) Granzyme B (GzmB) and Blimp-1 YFP expression in CD8 T cells from dLNs and lesions from Blimp-1 reporter mice infected with *L. major* for one week. (c) Schematic representation of OOD^{cre}Blimp-1$^{flox/flox}$ mice. (d) OOD^{cre}Blimp-1$^{flox/flox}$ mice were infected with *L. major* for one week when daily tamoxifen injections commenced. Mice were euthanized at week two post-infection. GzmB expression of lesional CD8 T cells in tamoxifen-treated and untreated mice. Data from two independent experiments combined. *P ≤ 0.05, **P ≤ 0.01, and ****P ≤ 0.0001.

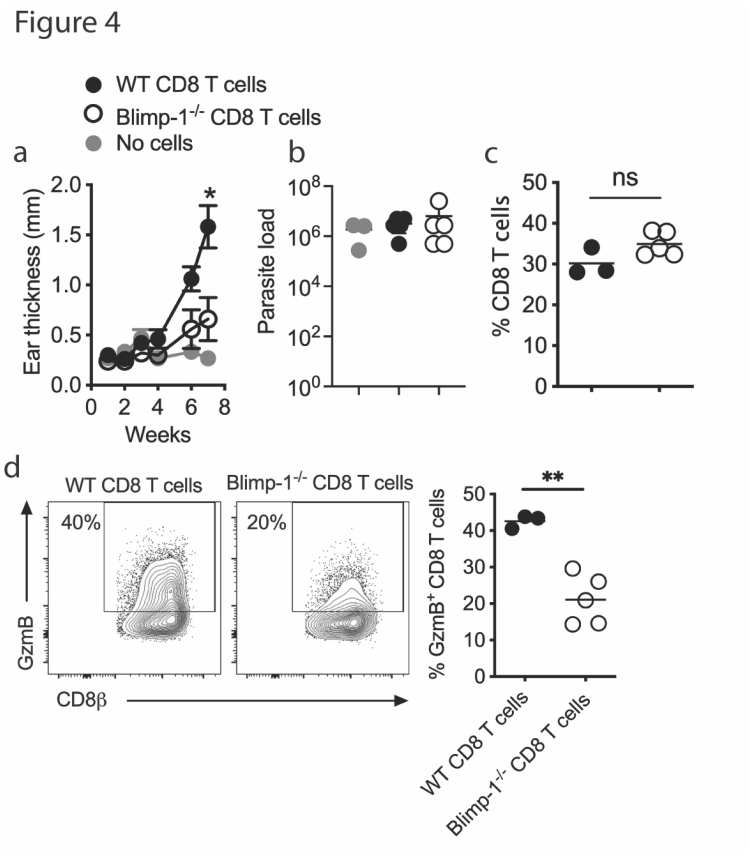

Fig 4. Blimp-1 expression is required for CD8 T cell-mediated disease.

RAG$^{-/-}$ mice were infected with *L. braziliensis* and reconstituted with CD8 T cells purified from WT or Blimp-1^{cKO} mice. (a) Ear thickness and (b) parasite numbers in lesions at seven weeks of infection. (c) CD8 T cell frequency and (d) GzmB expression by CD8 T cells in lesions were assessed directly ex vivo by flow cytometry seven weeks after infection. Data represent 3 individual experiments with 3-5 mice per group. *P ≤ 0.05 and **P ≤ 0.01. ns = non-significant

Figure 5

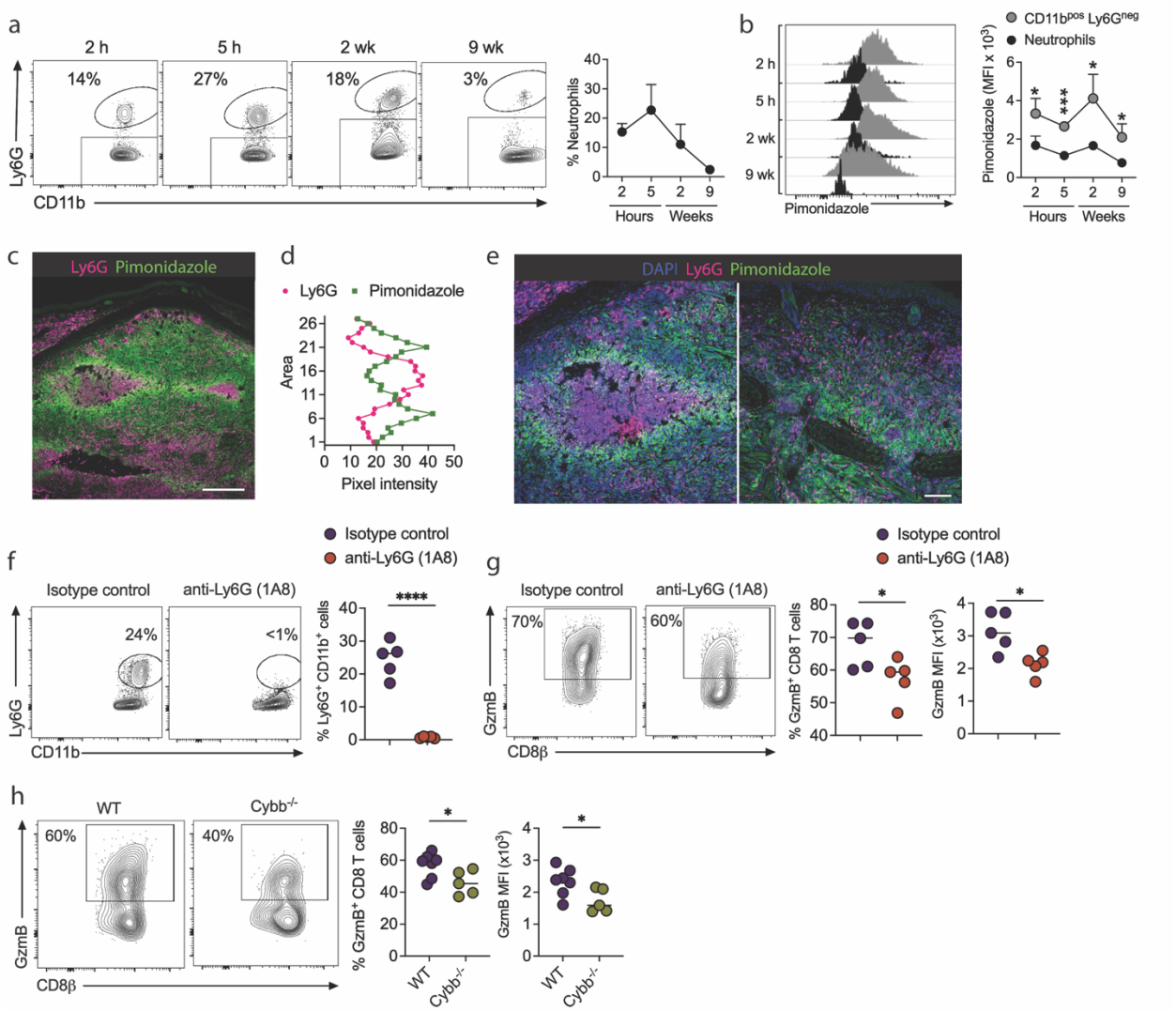

Fig 5. Neutrophils consume oxygen from lesions and stimulate granzyme B expression in CD8 T cells.

(a-b) C57BL/6 mice infected with *L. major* received pimonidazole one hour before euthanasia at two hours, five hours, two weeks, and nine weeks. (a) Frequency of neutrophils in lesions and (b) pimonidazole expression in neutrophils ($CD11b^{+}Ly6G^{pos}$) and other myeloid cells ($CD11b^{+}Ly6G^{neg}$) in lesions. (c) Confocal microscopy of one representative image of Ly6G (pink) and pimonidazole (green) staining in the skin infected for two weeks. Scale bar = 200 µm. (d) Pixel intensity of pimonidazole and Ly6G based on 27 regions (Fig. S3). (e) Confocal microscopy of two representative images of nuclear (DAPI) staining (blue), Ly6G (pink), and pimonidazole (green) in lesions infected for two weeks. Scale bar = 100 µm. (f-g) C57BL/6 mice infected with *L. major* were injected every three days with anti-Ly6G (clone 1A8) or isotype control until euthanasia at two weeks post-infection. Frequency of (f) neutrophils in lesions. (g) Granzyme B (GzmB) frequency and mean fluorescence intensity (MFI) in CD8 T cells in lesions. (h) Granzyme B frequency and MFI in CD8 T cells in the lesions of WT or $Cybb^{-/-}$ mice infected with *L. major* for two weeks. *$P \leq 0.05$, ***$P \leq 0.001$ and ****$P \leq 0.0001$.

Figure 6

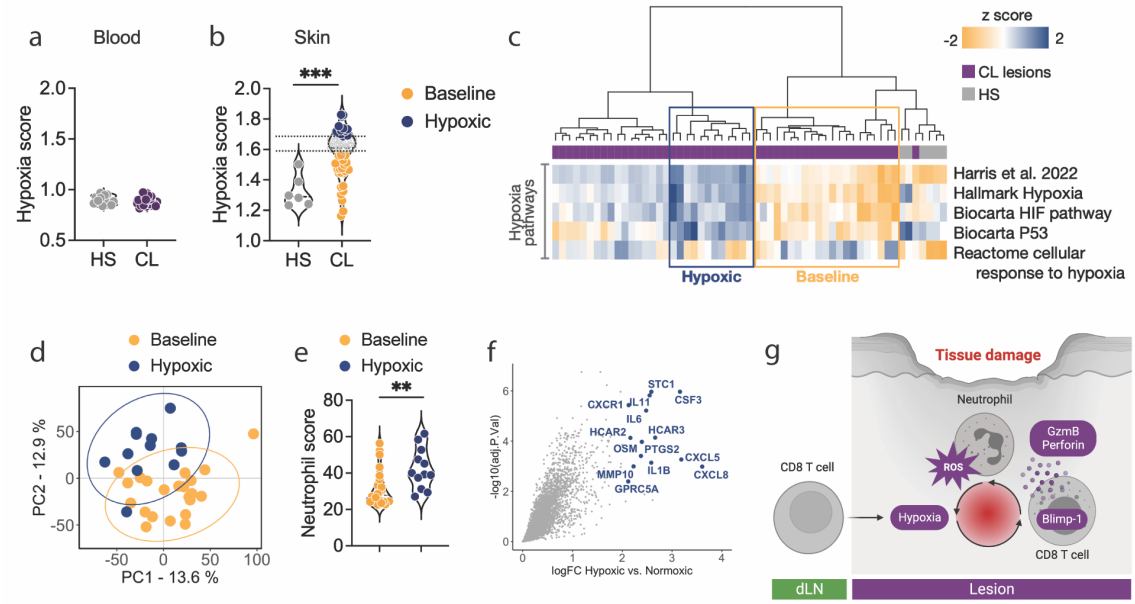

Fig 6. The degree of hypoxia-related gene expression is associated with the presence of neutrophils in patients.

(a) Hypoxia score calculated in the blood from healthy subjects (n=14) and patients (n=50); (b) human intact skin (n=6) and cutaneous leishmaniasis lesions from patients (n=51) based on the Harris et al. hypoxia-gene signature. (c) Unsupervised hierarchical clustering classified human skin samples in 'baseline' and 'hypoxic' lesions according to their hypoxia-gene phenotypes. (d) Principal Component Analysis (PCA) of baseline and hypoxic cutaneous leishmaniasis lesions. (e) Neutrophil abundances estimated by Microenvironment Cell Populations (MCP) counter. Wilcoxon was used for statistical analysis. (f) Scatter plot showing differential gene expression analysis between hypoxic vs. baseline lesions (FDR>0.01 and FC=1.5). In blue are the top DGEs from this analysis. (g) Model summarizing our findings. **$P \leq 0.01$, and ***$P \leq 0.001$. HS = Healthy subjects. CL = cutaneous leishmaniasis. FDR = false discovery rates. FC = fold change.

Figure S1

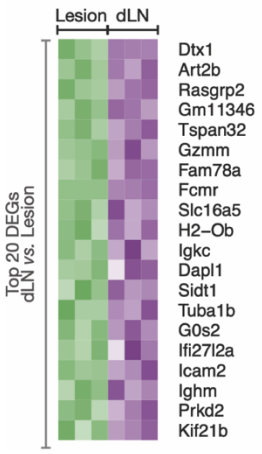

Supp. Fig. 1. Genes overexpressed in CD8 T cells purified from dLNs compared to lesions.

C57BL/6 mice were infected with *L. major*, and at the peak of the lesion, antigen-experienced ($CD44^{high}$) CD8 T cells were purified by flow cytometry cell sorting and used for RNA-seq. Heat map of top 20 differentially expressed genes overexpressed in CD8 T cells purified from dLN compared to lesions.

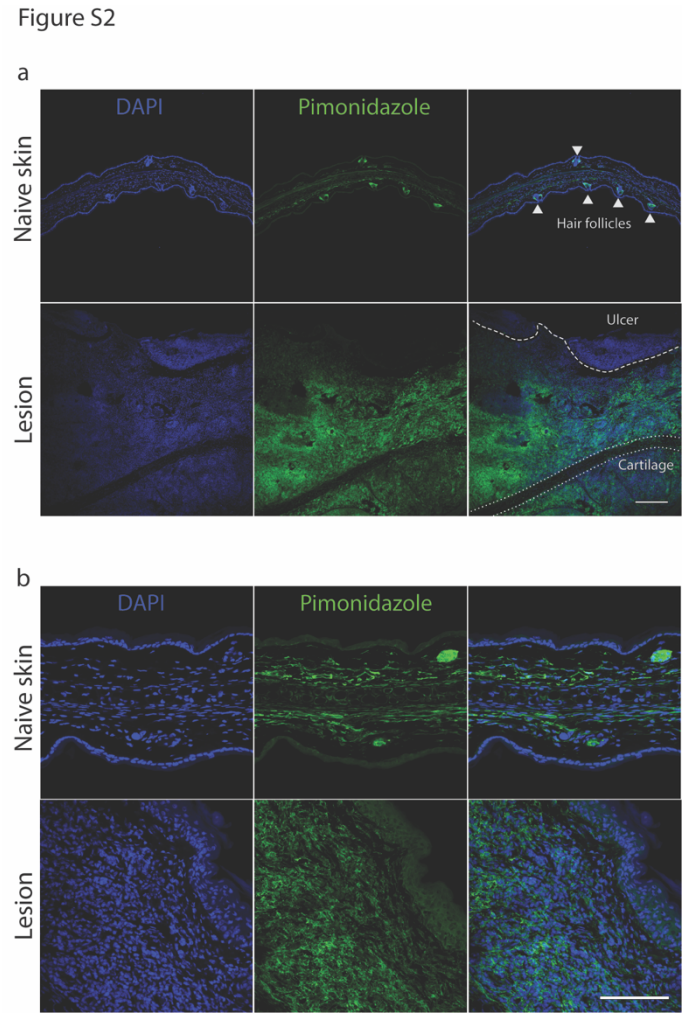

Supp. Fig. 2. Pimonidazole expression in *Leishmania*-infected skin.

C57BL/6 mice infected with *L. major* received pimonidazole one hour before euthanasia at two weeks. (a) Individual images from confocal microscopy (Fig. 2a). Nuclear (DAPI) staining (blue) and pimonidazole (green) in contralateral ears (naïve skin) and infected ears (lesions) for two weeks. Scale bar = 200 µm. (b) Individual images from confocal microscopy (Fig. 2b). Nuclear (DAPI) staining (blue) and pimonidazole (green) in contralateral ears (naïve skin) and infected ears (lesions) for two weeks. Scale bar = 100 µm.

Figure S3

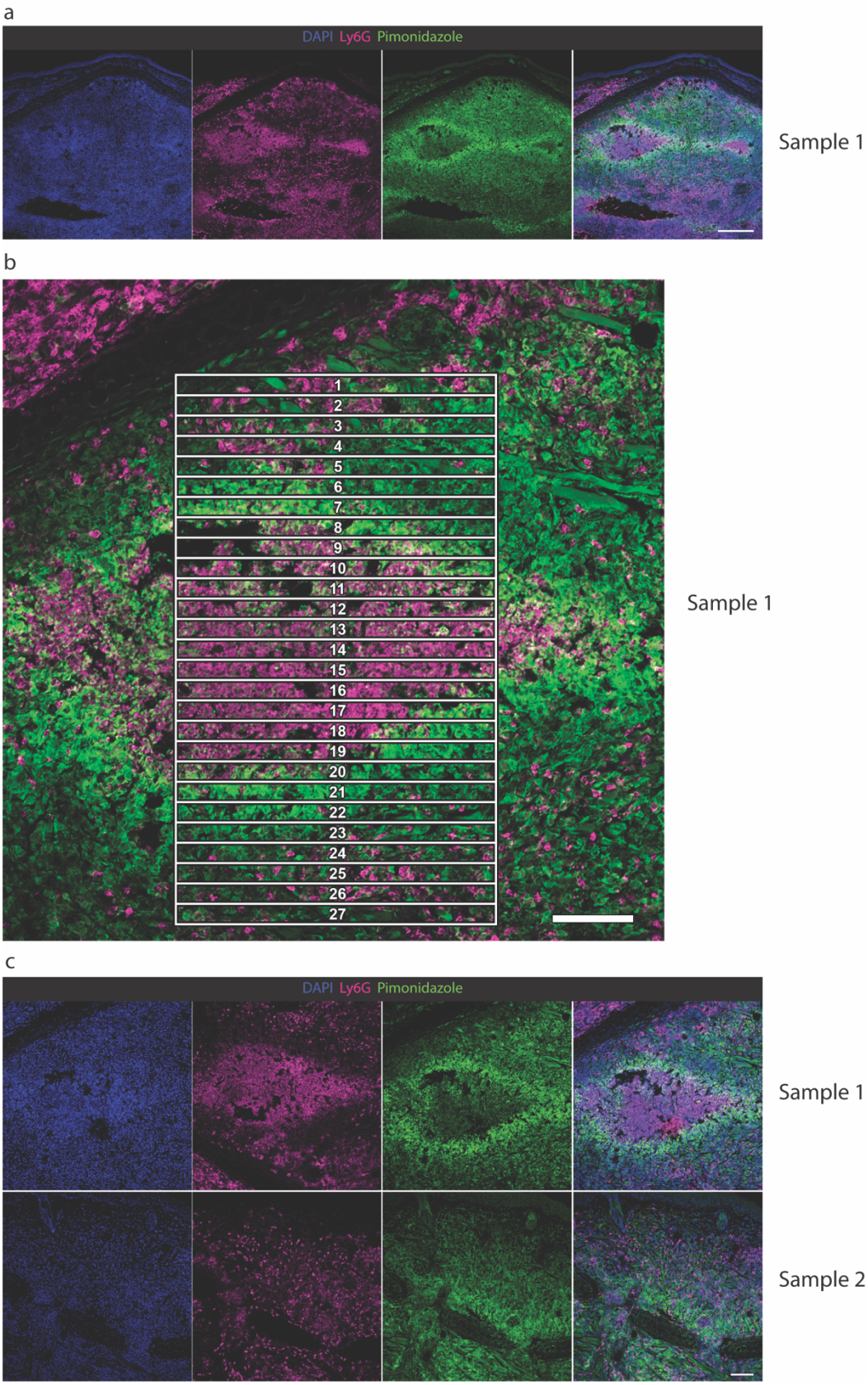
a
DAPI Ly6G Pimonidazole
Sample 1
b
1
2
3
4
5
6
7
8
9
10
11
12
13
14
15
16
17
18
19
20
21
22
23
24
25
26
27
Sample 1
c
DAPI Ly6G Pimonidazole
Sample 1
Sample 2

942 Supp. Fig. 3. Neutrophil and pimonidazole expression in *Leishmania*-infected skin.
943
944 C57BL/6 mice infected with *L. major* received pimonidazole one hour before euthanasia at two weeks. (a)
945 Individual images from confocal microscopy (Fig. 5c). Nuclear (DAPI) staining (blue), Ly6G (pink), and
946 pimonidazole (green) in the skin infected for two weeks. Scale bar = 200 μm. (b) Confocal microscopy image was
947 divided into 27 regions to measure the pixel intensity of Pimonidazole (green) and Ly6G (pink) shown in Fig. 5d.
948 Scale bar = 100 μm. (c) Individual images from confocal microscopy (Fig. 5e). Nuclear (DAPI) staining (blue),
949 Ly6G (pink), and pimonidazole (green) in the skin infected for two weeks. Scale bar = 100 μm.
950